Geodiversity of the Southern Barrington Tops Lava Field, New South Wales: A Study in Petrology and Geochemistry

M.C. Bruce

Department of Industry and Investment NSW – Mineral Resources, WB Clarke Geoscience Centre, Londonderry 2753, Australia.

Bruce, M.C. (2011), Geodiversity of the southern Barrington Tops Lava Field, New South Wales: A study in petrology and geochemistry. *Proceedings of the Linnean Society of New South Wales* **132**, 55-69.

The Barrington Tops lava field lies within the Barrington Tops National Park and State Forests north of the Hunter River Valley and west of Gloucester in eastern NSW. Mapping in the southern lava field has identified 33 basaltic flows each 10-20m thick and separated by agglomerate or by sub-horizontal palaeosols. Petrography and whole-rock geochemistry indicate basanites dominate the stratigraphic sequence, with subsidiary alkali basalts, pyroxene-phyric basalts (ankaramites) and tholeiites. Alkali gabbros form intrusions high in the sequence and represent conduits for surface lavas. Modelling of major and trace elements from the alkaline rocks reveal a co-genetic relationship, chiefly controlled by a low pressure olivine + plagioclase mineral assemblage. Incompatible trace elements suggest low degree melting of an enriched mantle source with entrained amphibole-enriched sub-continental lithospheric mantle. A more depleted mantle component may have contributed to the tholeiites. These southern findings are consistent with observations in the northern lava field, and help to model evolution of the Barrington Tops volcano. Topographic inversion has contributed to geomorphological features which support diverse floral and faunal communities. Such diversity is underpinned by the geology and in particular the lava field, which shaped the natural landscape, provides fertile soils and releases gem-quality sapphires, zircons and rubies.

Manuscript received 1 November 2010, accepted for publication 20 April 2011.

KEYWORDS: Barrington Tops, basalt, geochemistry, geodiversity, lava field, New South Wales, petrology,

INTRODUCTION

Barrington Tops is located approximately 100km north-northwest of Newcastle, New South Wales (Fig. 1; inset). The region is dominated by a plateau of average elevation approximately 1500m above sea level with a relief of over 1100m to the valley floors. Barrington Tops is rugged, heavily vegetated and incorporates the Barrington Tops National Park and several surrounding State Forests. Both the National Park and State Forests are well known for recreational purposes that derive from the environmental diversity and geomorphology – both dependent on the underlying geology – of this remarkable region.

The Barrington Tops lava field has a K-Ar age of 59 to 44 Ma (Wellman et al. 1969; Sutherland and Fanning 2001), although more recent fission track and U-Pb dating of zircons suggests that parts of the field were active for over 55 million years, until 4 Ma (Roberts et al. 2004). The volcanic field consists predominately of alkali basaltic rocks, with some olivine tholeiites at the base of the sequence (Mason 1982). Following Mason's (1982) interpretation of the basalts as flows, Pain (1983) envisaged that they were derived from a shield volcano, an idea supported by subsequent authors (O'Reilly and Zhang 1995; Sutherland and Fanning 2001; Sutherland and Graham 2003). The Cenozoic lavas in part overlie Late Permian granitoids which were emplaced at high crustal levels (3-7 km: Eggins 1984) and partly within low grade metamorphosed Carboniferous and Devonian sediments (Mason and Kavalieris 1984) of the New England Orogen that the granites intrude.

In this paper, I present data (collected in 1995 during my Honours thesis) from the southern part of the volcanic field (Fig. 1), an important addition to the literature as most data for these Paleocene/Eocene (51 to 59 Ma) basalts come from the northern side (Wellman et al. 1969; Mason 1982; Pain 1983; O'Reilly and Zhang 1995; Sutherland and Fanning 2001). The southern lavas range from SiO_2 -deficient basanites, akali basalts and rare trachybasalts to SiO_2

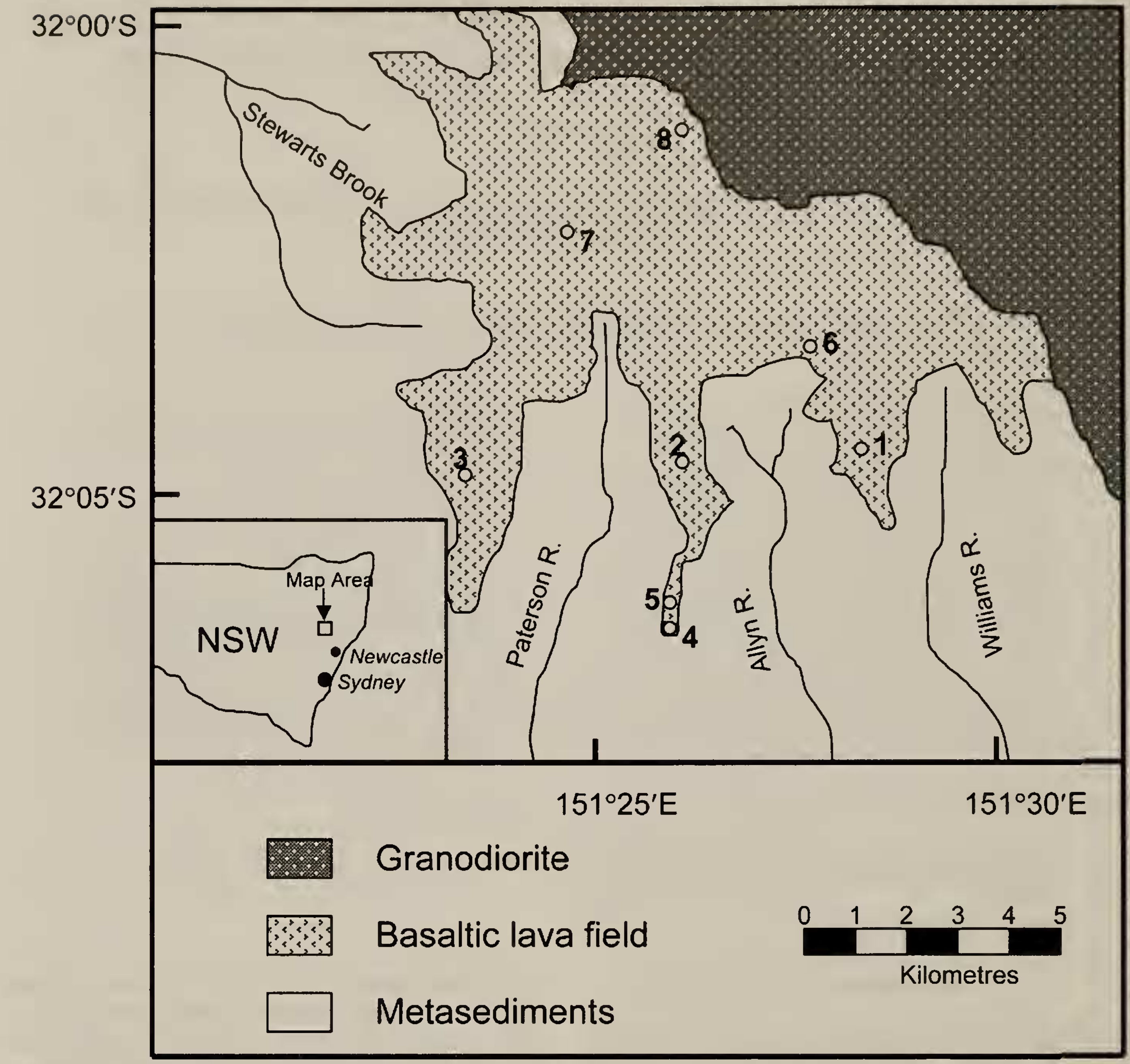

Figure 1. Simplified geological map of the southern Barrington Tops lava field. Numbered points refer to localities mentioned in the text: 1, Williams Range (Careys Peak Trail); 2, Allyn Range; 3, Mount Royal Range; 4, Mt Allyn; 5, Mt Lumeah; 6, Careys Peak; 7, Mt Barrington; 8, Barrington Falls. Inset indicates the map area within NSW.

saturated tholeiites, interspersed with pyroxene-phyric flows (ankaramites) and alkali gabbros.

STRATIGRAPHY

Local stratigraphy in the southern Barrington Tops basaltic field has been determined from detailed petrological study of individual lava flows from type sections exposed in several localities along the Careys Peak Trail, Mounts Allyn, and Lumeah and the Barrington Tops plateau (Fig. 1). Correlations between sites were carried out topographically because of the sub-horizontal nature of the basalt and a similar topographic height of the basalt-metasediment contact. This contact occurs at approximately 920m above sea level.

Fig. 2 is a stratigraphic sequence of the lavas differentiated on petrological and chemical criteria rather than on individual flows. The base of the sequence consists of a thin layer of alkali basalts (~20m thick) and tholeiites (~110m thick), with basanites dominating the middle section (> 200m thick). Interrupting the continuity of the basanites is a relatively thin succession of trachybasalts (~30 m thick). The upper part of the sequence comprises

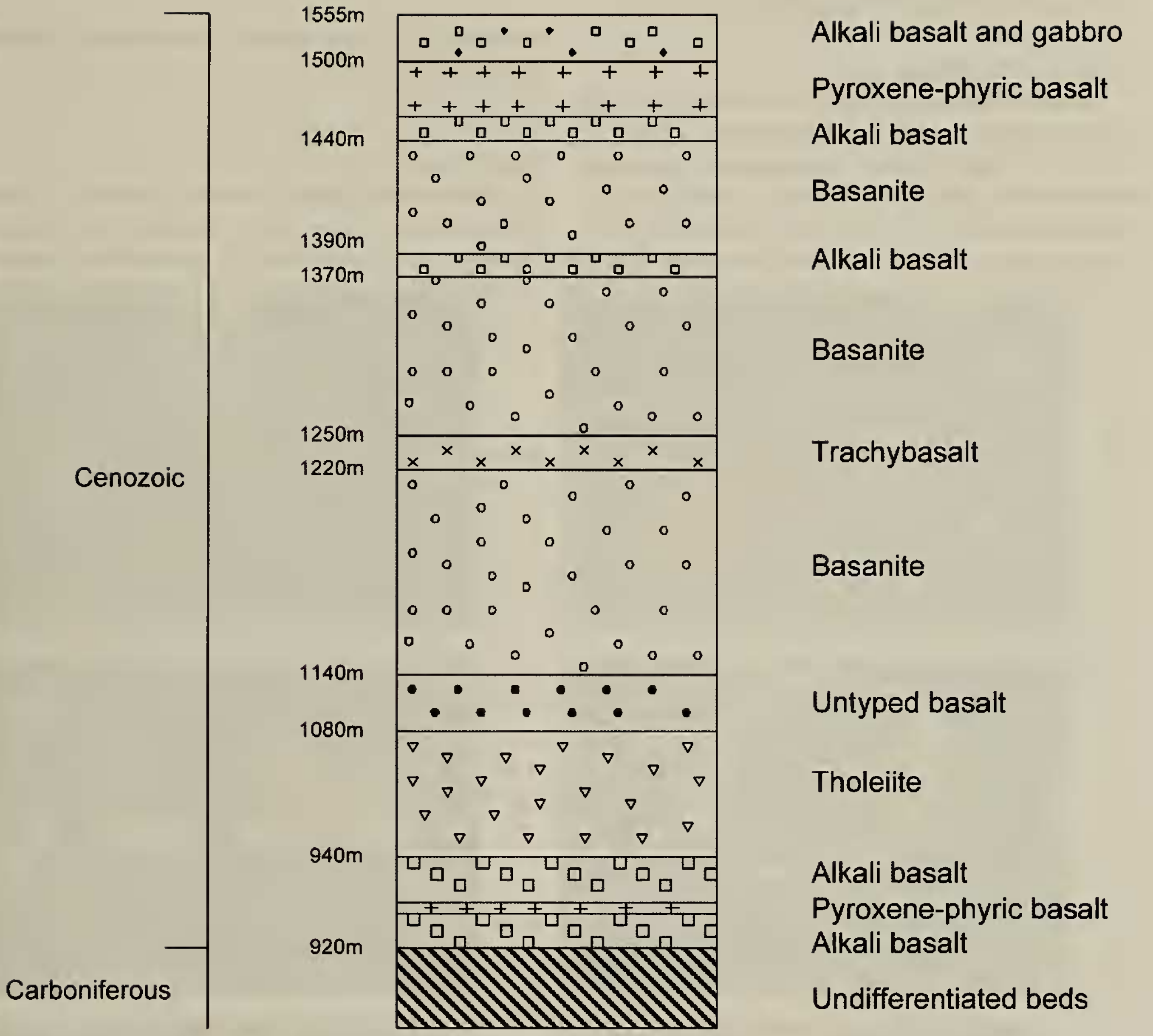

Figure 2. Volcanic stratigraphy for the southern part of the lava field. Delineations are based on changes in rock-type rather then individual flows. In all 33 flows are exposed through 630m of topographic relief. Numbers refer to elevation above sea level.

alternating successions of alkali basalt and basanite (~185m thick). Pyroxene-phyric basalt (ankaramite) occurs as thin layers both at the base and the top of the sequence in close association with the alkali basalts.

In all 33 individual flows are found to make up the sequence exposed through 630m of relief. Most volcanic flows are identified by the presence of an agglomerate/breccia up to 3 metres thick, which – given its regular occurrence every 10 to 20 metres in the succession – is interpreted to represent either the top or base of individual flows. Some volcanic flows, however, are conspicuous by the absence of the agglomerate. These flows are usually the most vesicular (due to passively expelled volatiles) and are commonly separated by sub-horizontal palaeosols, indicating a temporary cessation of volcanism with weathering and erosion.

Alkali gabbro (teschenite) is also present on the Barrington Tops plateau at Careys Peak and to the south of Mount Barrington above an apparent magma chamber (Wellman 1989). The alkali gabbro was originally noted by Benson (1912) and interpreted as intrusive dykes or sills. Measurement of magnetic anisotropy from one basanite (Barrington Falls) and one tholeiite (Williams Range) indicates that the dominant lineation in these samples strikes approximately north-south and northwest-southeast respectively. Projection of these directional lines intersects on the alkali gabbro to the south of Mount Barrington (Bruce 1995), suggesting that this intrusive body represents remnant vents from which the lava was extruded.

PETROGRAPHY AND MINERAL CHEMISTRY

Analytical Techniques

Minerals were analysed for major elements using a Cameca SX50 Electron Microprobe calibrated with natural and synthetic materials with a general precision ≤ 1%. Analytical conditions were optimised for a standard silicate run using a 15kV accelerating voltage and a 20nA focussed electron beam for all elements, with the exception of K and Na for which a broader (10nA) beam was used. Routine analyses were obtained by counting 30s at peak and 5s on background.

Alkali Basalt (Fig. 3a)

The alkali basalts are fine-grained in hand specimen with scattered phenocrysts of greenish olivine up to 5mm in size. In thin section, the fine-

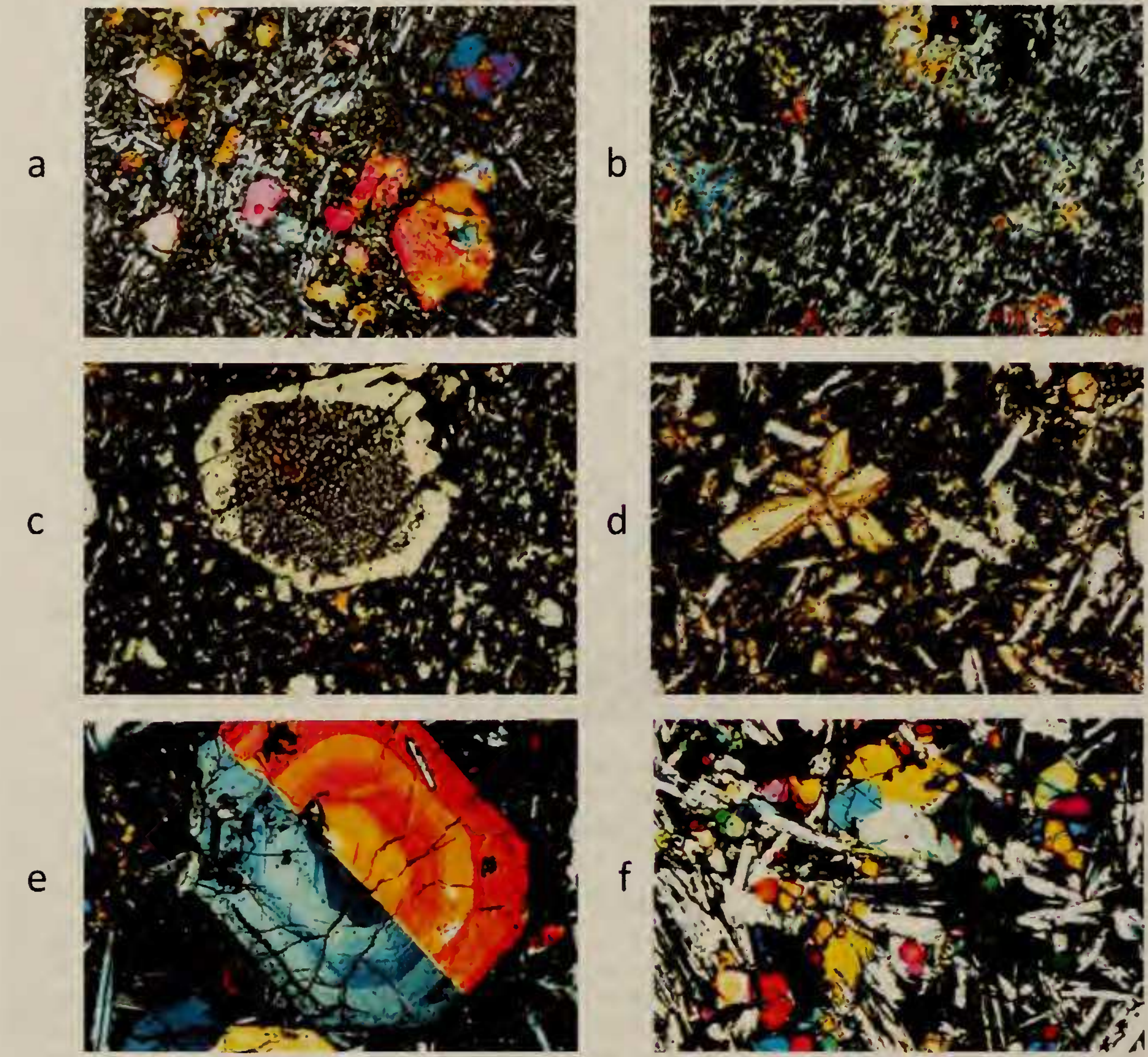

Fig. 3, (a). Photomicrograph (cross polarisation) of an alkali basalt illustrating olivine phenocrysts scattered throughout the groundmass with abundant plagioclase laths. Magnification x 2.5. (b). Photomicrograph (cross polarisation) of a tholeiite displaying ophitic texture defined by plagioclase laths embedded in clinopyroxene. Magnification x 2.5. (c). and (d). Photomicrographs (plane polarisation) from basanites demonstrating three different clinopyroxene textures. Top photo illustrates a sieve-textured proxene (top centre). Bottom photo shows pyroxene crystals in a radiating texture (left centre) and small euhedral phenocrysts (pinkish tinge). Magnification x 6.3. (e). Oscillatory zoning in a twinned Ti-rich diopside phenocryst from a pyroxene-phyric basalt. Cross polarisation. Magnification x 6.3. (f). Photomicrograph of a holocrystalline alkali gabbro dominated by plagioclase laths, olivine and clinopyroxene crystals. Cross polarisation.

grained groundmass is composed of intergranular olivine, clinopyroxene, plagioclase, Fe-Ti oxides and intersertal glass. Subhedral phenocrysts and microphenocrysts of olivine are present (0.1-2mm) as are abundant calcic plagioclase laths (0.2mm). The larger olivine phenocrysts are commonly zoned from a relatively Mg-rich core (Fo_{72}) to more Fe-rich rims (Fo_{63}). Clinopyroxene is notable in its absence as a phenocryst phase and is restricted to the groundmass where it is of diopside composition ($En_{38}Fs_{14}Wo_{48}$). Zeolites are also present as a minor secondary phase and occur as amygdules (0.2mm).

Tholeiite (Fig. 3b)

The tholeiites are very fine-grained and dark grey in hand specimen. In outcrop they are horizontally (?flow) layered. In thin section they are ophitic to subophitic in texture and consist of clinopyroxene and olivine phenocrysts in a groundmass of plagioclase laths, clinopyroxene and Fe-Ti oxides. Rare, prism-shaped plagioclase phenocrysts (~0.4mm) are also present. The plagioclase laths with an average length of 0.1mm are embedded in augite crystals which average 0.7mm in size. Olivine microphenocrysts, however, do not contain any plagioclase inclusions. Intersertal glass and chlorite is evident in the groundmass.

Basanite (Figs 3c and 3d)

The basanites are very fine-grained in hand specimen with small phenocrysts (medium 0.5mm) of olivine and clinopyroxene. In thin section, olivine (Fo_{84-90}) is the most abundant phenocryst, averaging 0.5mm with a maximum of 2mm. Olivine microphenocrysts (0.2mm) and similar sized calcic plagioclase laths (An_{60-71}) are dominant in a fine-grained groundmass of intergranular and interstitial clinopyroxene, olivine, magnetite, calcic plagioclase and mesostasis feldspar. Zeolites usually occur as small amygdules but are also observed as large crystals up to 2mm in size. Glomeroporphrytic aggregates of olivine are common in some samples.

Three types of clinopyroxene phenocrysts occur within the basanites: 1. euhedral pyroxene phenocrysts (average 0.8mm) in which the cores are sieve-textured consisting of probable glass and clinopyroxene, which could not satisfactorily be analysed, and rims that are glass free and composed of diopside ($En_{39}Fs_{10}Wo_{51}$); 2. small (0.3mm) radiating crystals that are zoned from a diopside core ($En_{38}Fs_{13}Wo_{49}$) to a Ti-rich aluminium diopside rim ($En_{32}Fs_{16}Wo_{52}$); 3. large (up to 0.9mm) subhedral to euhedral clinopyroxene phenocrysts zoned from cores of $En_{39}Fs_{13}Wo_{48}$ to rims of Ti-rich aluminium diopside ($En_{33}Fs_{15}Wo_{52}$). The first type of phenocryst is interpreted to represent slow growth of clinopyroxene in which the core has trapped melt before crystallising the outer margin probably during quenching. The second type represents a snapshot of the early stages of pyroxene growth. Further growth of this type has resulted in the third type.

In addition, clinopyroxene xenocrysts are evident in some samples. These are commonly large in size (up to 9mm) and sub-rounded in shape. A gabbroic enclave (5mm) that occurs in one sample consists of clinopyroxene ($En_{37}Fs_{16}$Wo47), orthopyroxene ($En_{59}Fs_{41}$) and calcic plagioclase ($An_{80}Ab_{20}$). The presence of orthopyroxene in apparent equilibrium with clinopyroxene suggests that the enclave was formed under high pressure and transported to the surface rapidly to prevent resorption during ascent (T. Green pers. comm. 1995). This is supported by aluminium stoichiometry in the clinopyroxenes where $Al^4:Al^6 = 1.8$, suggesting crystallisation pressures >1 GPa (Thompson 1974; Wass 1979) or >35 km in depth. However, the relatively low Al_2O_3 content of the co-existing orthopyroxenes (2.2 wt%) is not consistent with an upper mantle origin (Binns et al. 1970) and therefore probably crystallised at crustal pressures.

Pyroxene-phyric Basalt (Fig. 3e)

These basalts (ankaramites) are conspicuous in hand specimen due to an estimated 30-40 percent of large (up to 10mm) clinopyroxene megacrysts. In thin section, the megacrysts are diopside in composition and display strong oscillatory zoning with Mg-rich cores ($En_{40}Fs_{12}Wo_{48}$) and Fe-Ca-rich rims ($En_{34}Fs_{15}Wo_{51}$). They are also Ti-rich with 2-3 wt% TiO_2. The megacrysts contain various inclusions of diopside ($En_{40}Fs_{11}Wo_{49}$), olivine (Fo_{74}), plagioclase ($An_{66}Ab_{34}$) and Ti-rich magnetite. Olivine phenocrysts (1-2mm) zoned from cores of Fo_{74} to rims of Fo_{64} and plagioclase laths ($An_{66}Ab_{34}$) up to 2mm, are abundant and embedded in a fine hypocrystalline groundmass of clinopyroxene ($En_{35}Fs_{18}Wo_{47}$), olivine (Fo_{62}), calcic plagioclase and magnetite - ulvöspinel.

Both zoning in the phenocrysts and megacrysts and inclusions in the megacrysts would suggest variable crystal growth rates, typical of cumulative textures.

Alkali Gabbro (Fig. 3f)

The alkali gabbros are holocrystalline and consist of Ti-rich diopsides up to 5mm in size and 2mm olivine phenocrysts. The diopsides are zoned from $En_{42}Fs_{11}Wo_{47}$ to $En_{37}Fs_{16}Wo_{47}$ with entrained plagioclase (An_{62}) and magnetite - ulvöspinel inclusions. Olivine phenocrysts commonly form a glomeroporphrytic texture and can be strongly zoned from Fo_{71} cores to more Fe-rich (Fo_{58}) rims. Large plagioclase (An_{60}) laths up to 3mm are abundant and set in a coarse (>0.5mm) groundmass of clinopyroxene ($En_{35}Fs_{18}Wo_{47}$), forsterite, mesostasis feldspar, magnetite - ulvöspinel, analcime and apatite needles.

WHOLE-ROCK COMPOSITIONS

Analytical Techniques

Samples were crushed in a TEMA tungsten carbide mill. Major elements were determined using glass fusion discs (Norrish and Hutton 1969) by X-ray Fluorescence (XRF). The instrument used was a Siemen's SRS-1. Calibration was by means of international rock standards and well-calibrated internal standards. All samples were run in duplicate. Trace elements were analysed by XRF using pressed-powder pellets. Mass absorption corrections were applied (Norrish and Chappell 1977). All samples were analysed in duplicate, using international rock standards. FeO was determined by HF digestion and titration with Ceric sulphate. Estimates of precision based on USGS standards BCR-1 and GSP-1, and NIM standard NIM-G are: Major elements; $< \pm 1\%$ relative at > 10 wt% levels; Mn, P, Mg, Na $\leq 2\%$ relative for BCR-1: Trace elements; $\leq 1\%$ relative at 100ppm levels; ± 10ppm for < 100ppm.

Results

Selected bulk-rock data representing each described rock-type are presented in Table 1. The results for all samples analysed are tabulated in the Appendix (Table A1).

Major Elements

The majority of sampled basalts are undersaturated basanites and alkali basalts according to the classification of Le Bas et al. (1986), although one tholeiite and one trachybasalt has also been sampled (Fig. 4). The pyroxene-phyric basalt and the alkali gabbro when considered as plutonites plot as monzogabbro and gabbro respectively using the scheme of Middlemost (1985; not shown). Major elements versus Mg# [$100Mg/(Mg + Fe^{2+})$] are plotted in Fig. 5 for all samples except the tholeiite. Although some diagrams show substantial scattering, both Al_2O_3 and MgO display strong, coherent trends. This would suggest that all alkaline magmas are related petrogenetically via processes dominated by compositions that concentrate the elements Al_2O_3 and MgO (fractionation/accumulation, partial melting, mixing). Overall there is an increase in TiO_2, Al_2O_3, FeOt (total iron) and K_2O and a decrease in MgO and CaO with increasing fractionation (decrease in Mg#). A positive correlation between CaO/Al_2O_3 and Mg# for the basanites and alkali basalts with Mg# <70 would indicate clinopyroxene fractionation in these rocks.

Trace Elements

Plots of the compatible elements Ni and Cr versus Mg# (Fig. 6) define a strong, positive correlation for the former but a more scattered relationship for the latter. This, combined with a similar MgO trend, suggests that olivine fractionation was the dominant process by which the alkaline magmas were related. Clinopyroxene may not have been a significant fractionating phase in controlling magma composition in the basanites and alkali basalts given the reasonably constant Cr concentrations; although it could have been important in the evolution of the trachybasalts, pyroxene-phyric basalts and alkali gabbros.

Zr/Nb values are virtually constant within a magmatic suite as crystal fractionation and wall rock reaction have little effect on this ratio (Green 1992). This ratio does, however, increase with increasing degrees of partial melting, from values around 3-6 for oceanic island basalts (OIB) to > 30 for normal mid ocean ridge basalts (N-MORB) (Crawford et al. 1997). The alkaline magmas in the southern Barrington Tops lava field have Zr/Nb = 2-3, whereas the sampled tholeiite has a Zr/Nb value > 4. The higher ratio in the tholeiite could indicate either a different, or a heterogeneous, magma source. Furthermore, the source(s) for both magma lineages have Zr/Nb ratios typical of OIB. Multi-element diagrams for both the alkaline magmatic suite and the tholeiite are presented in Fig. 7. These plots are normalised to the average OIB values of Sun and McDonough (1989). Overall, the alkaline magmas have patterns and element concentrations similar to OIB. However, relative to the average OIB, the rocks are depleted in Rb, K, Zr, Ti and Y and enriched in Ba, Nb, Sr and P. The tholeiite follows a similar pattern but has concentrations more akin to enriched mid ocean ridge basalt (E-MORB) suggesting a slightly more depleted component in its source.

PETROGENESIS

Major and trace elements indicate that the alkaline magmas were strongly controlled by the fractionation of a phase dominated by MgO and Ni content and accumulation of a phase dominated by

Table 1 Selected major and trace element XRF analyses, southern Barrington lava field.

Sample	MU55361	MU55372	MU55418	MU55365	MU55369	MU55397
Barrington Tops 1:25k 9133-1-N	GR.492538	GR.553522	GR.560480	GR.500539	GR.502533	GR.555490
Rock type	Alkali basalt	Basanite	Tholeiite	Pyroxene-phyric basalt	Alkali gabbro	Trachybasalt
wt%						
SiO_2	47.44	44.16	49.15	45.25	48.9	46.1
TiO_2	1.97	2.53	1.49	2.55	2.3	2.65
Al_2O_3	14.49	14.54	16.42	16.01	16.38	15.97
Fe_2O_3	1.93	1.91	2.09	1.85	1.85	1.9
FeO	9.63	9.55	10.44	9.28	9.23	9.49
MnO	0.17	0.19	0.16	0.18	0.16	0.18
MgO	10.44	10.95	6.33	7.31	6.28	7.99
CaO	9.8	11.5	10.03	11.73	9.67	9.19
Na_2O	2.72	2.98	2.77	3.32	3.28	3.32
K_2O	1.11	0.85	0.52	1.77	1.24	1.78
P_2O_5	0.39	1.07	0.32	0.96	0.5	0.88
Total	100.09	100.23	99.74	100.21	99.79	99.45
CIPW norms						
Or	6.56	5.02	3.08	10.45	7.35	10.59
Ab	20.75	11.24	23.48	9.5	27.78	18.8
An	23.99	23.7	30.88	23.46	26.32	23.5
Ne	1.2	7.53	0	10.03	0	5.1
Di	18.06	21.75	14.17	23.64	15.42	13.96
Hy	0	0	15.28	0	1	0
Ol	22.06	20.88	6.54	13.33	13.96	18.29
Mt	2.8	2.76	3.04	2.68	2.69	2.77
Il	3.74	4.8	2.84	4.83	4.38	5.06
Ap	0.85	2.33	0.7	2.09	1.09	1.93
An/An+Ab	0.536	0.678	0.568	0.712	0.487	0.556
Mg/Mg+Fe^{2+}	0.659	0.672	0.519	0.584	0.548	0.600
ppm						
Ba	409	580	146	712	381	606
Rb	20	22	6	33	17	22
Sr	634	1146	412	1017	666	1328
Y	20	23	22	27	25	27
Zr	122	246	80	226	158	324
Nb	46	103	19	115	53	121
Th	1	6	0	7	1	3
Pb	5	3	3	3	5	2
Ga	19	20	21	23	24	19
Zn	90	80	80	76	84	83
Cu	43	51	71	62	43	33
Ni	171	177	208	82	52	107
V	228	243	192	240	219	195
Cr	351	337	294	112	84	115

Al_2O_3. In a basaltic system, the two phases likely to be involved are olivine and plagioclase respectively. However, Harker-style plots cannot preclude the importance of clinopyroxene as a fractionating phase. Therefore the mineral assemblages; olivine + plagioclase and olivine + plagioclase + clinopyroxene (amongst others) are tested below using the model of Pearce (1968). In this model, element ratios are used instead of oxide-oxide wt% diagrams as the latter may produce spurious correlations (Russell and Nicholls 1988; Rollinson 1993). These ratios are referred to as Pearce Element Ratios (PER) and are based on stoichiometry of the end-members of the mineral phases. The data almost always falls on a straight line (within analytical errors) and by applying a least squares linear regression technique, the slope

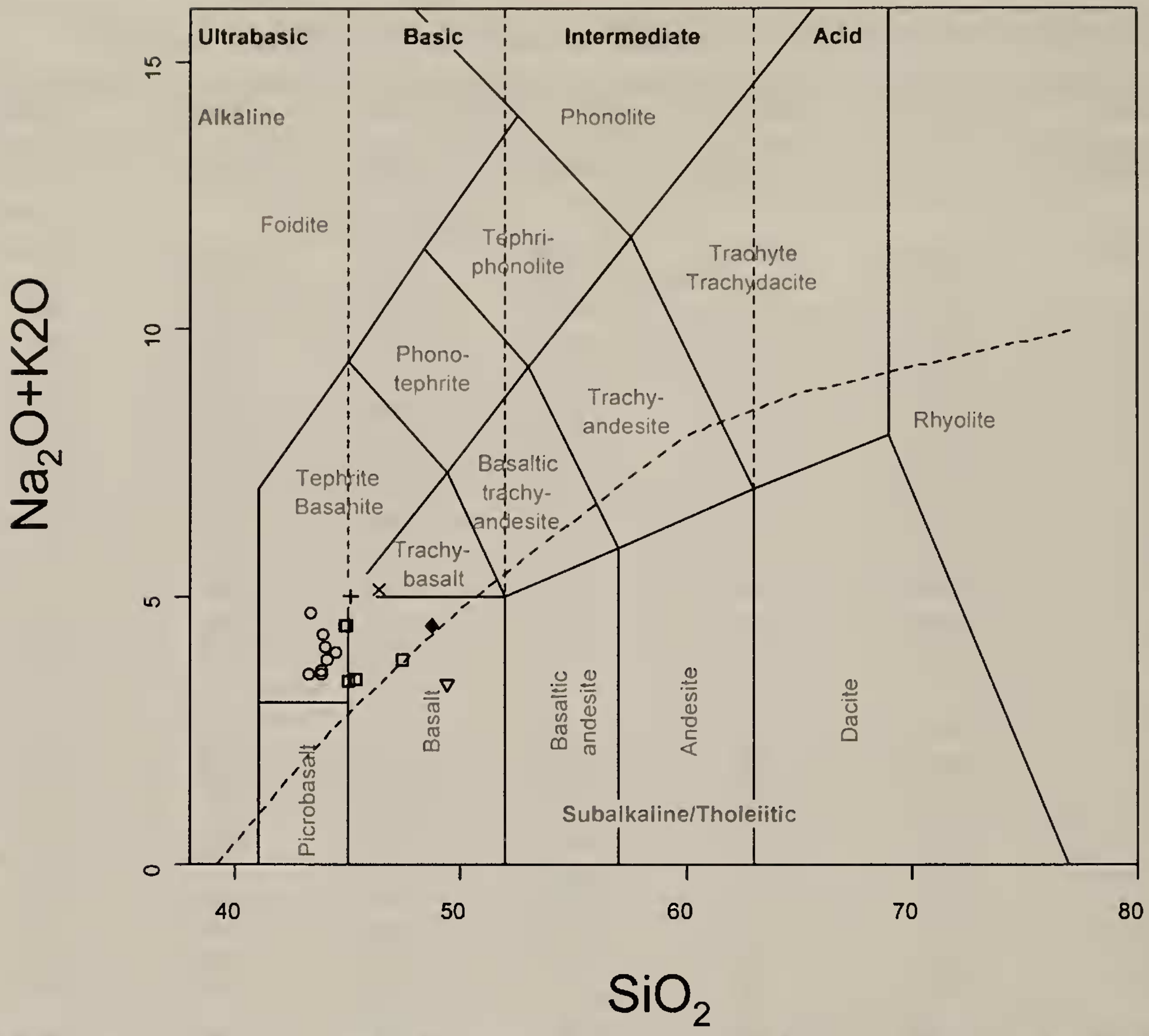

Figure 4. Rock classification diagram of Le Bas et al. (1986). Plotted are the various basaltic lithologies from the southern part of the lava field. Symbols: ○ = basanite; □ = alkali basalt; × = trachybasalt; + = pyroxene-phyric basalt; ◆ = alkali gabbro; ▽ = tholeiite.

of the line can be calculated. This slope reflects the stoichiometry of the minerals, which should equal one (2σ error) if the minerals tested for are in fact the phases involved in the differentiation of the magma. Fig. 8 presents PER diagrams for the following mineral assemblages within a basaltic system; olivine, clinopyroxene, plagioclase, olivine + clinopyroxene, olivine + plagioclase, olivine + clinopyroxene + plagioclase. The pyroxene-phyric basalt and the alkali gabbro have been removed from the model because of the abundance of large crystals that are highly likely to be cumulates from the magmas. The mineral assemblage olivine + plagioclase is the only assemblage that produces a slope of one (0.97) within the 95% confidence limit. Thus, the PER model validates the linear trends of MgO and Al_2O_3 observed in the Harker-style diagrams as fractionation/accumulation controlled. Despite the dominant assemblage of olivine + plagioclase, clinopyroxene must still have been involved in the fractionation process as phenocrysts of this mineral do occur in the basanites, trachybasalts, ankaramites and alkali gabbros.

The mantle reservoir for the alkaline magmas has been established as an OIB-type source. Greater enrichment in Nb, Sr and P coupled with depletions in Ti and Y than the average OIB can be explained by smaller degrees of partial melting of a fertile mantle source. However, simple melting models alone cannot explain the lower than expected depletions of Rb, K and Zr. O'Reilly and Zhang (1995) attributed similar Rb and K depletions from the western Barrington Tops lava field to the melting of metasomatised mantle in which residual amphibole was retained in the source. This explanation is also appropriate to the southern part of the lava field. The low Zr anomalies

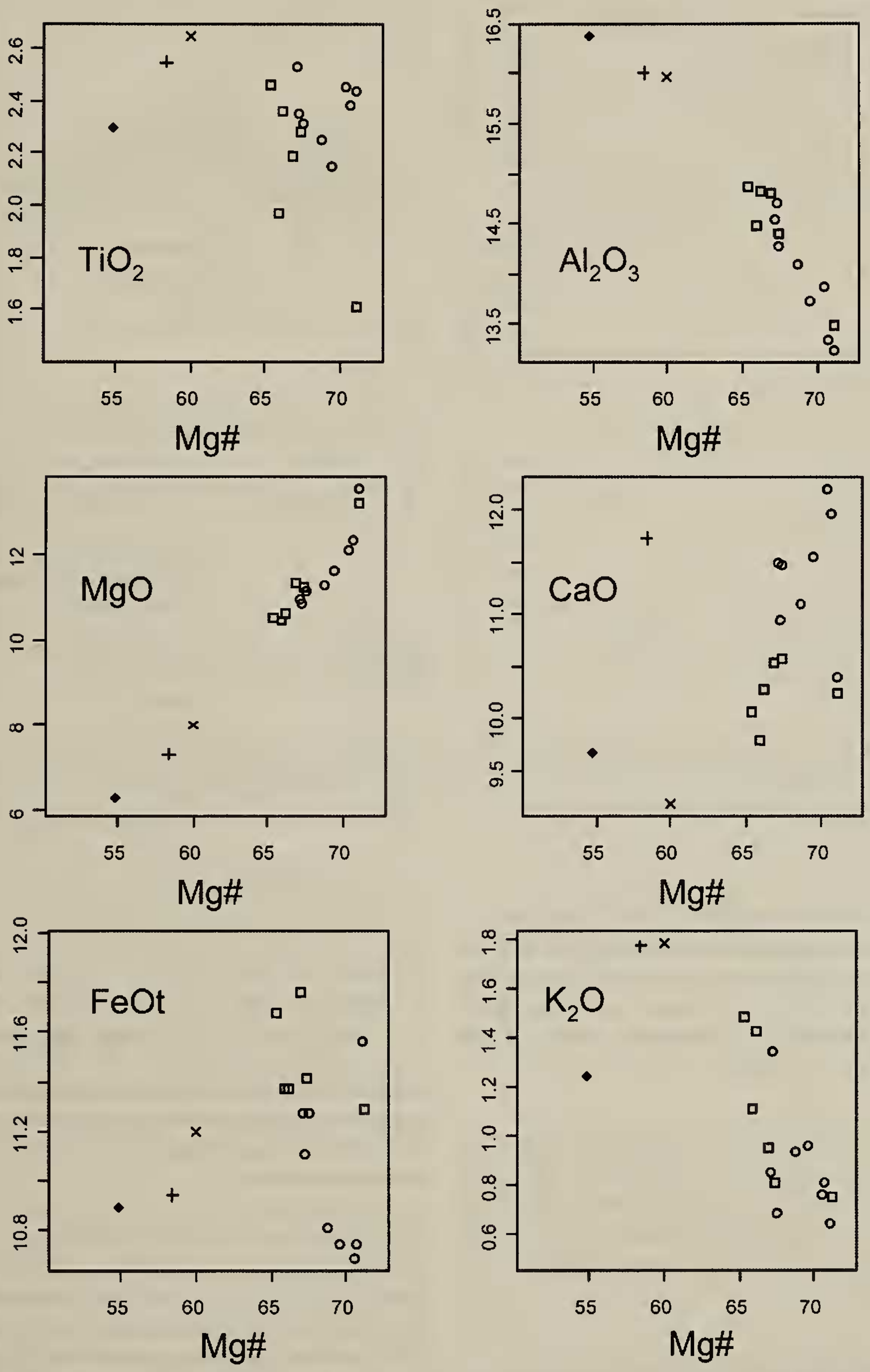

Fig. 5 Major elements (wt%) versus Mg# {100Mg/(Mg+Fe^{2+})}. Same symbols used as in Figure 4. Nb. Tholeiite is not plotted.

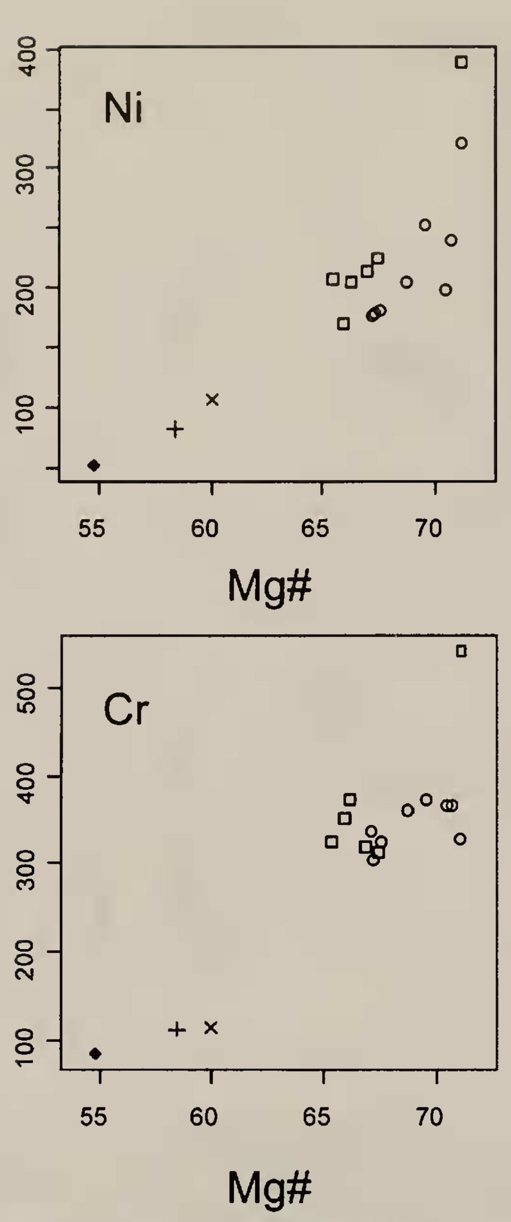

Figure 6 The compatible elements Ni and Cr (ppm) versus Mg#. Note that the alkali basalt with Ni > 300ppm and Cr > 500ppm has petrographic features indicative of cumulative olivine. Same symbols used as in Figure 4. Nb. Tholeiite is not plotted.

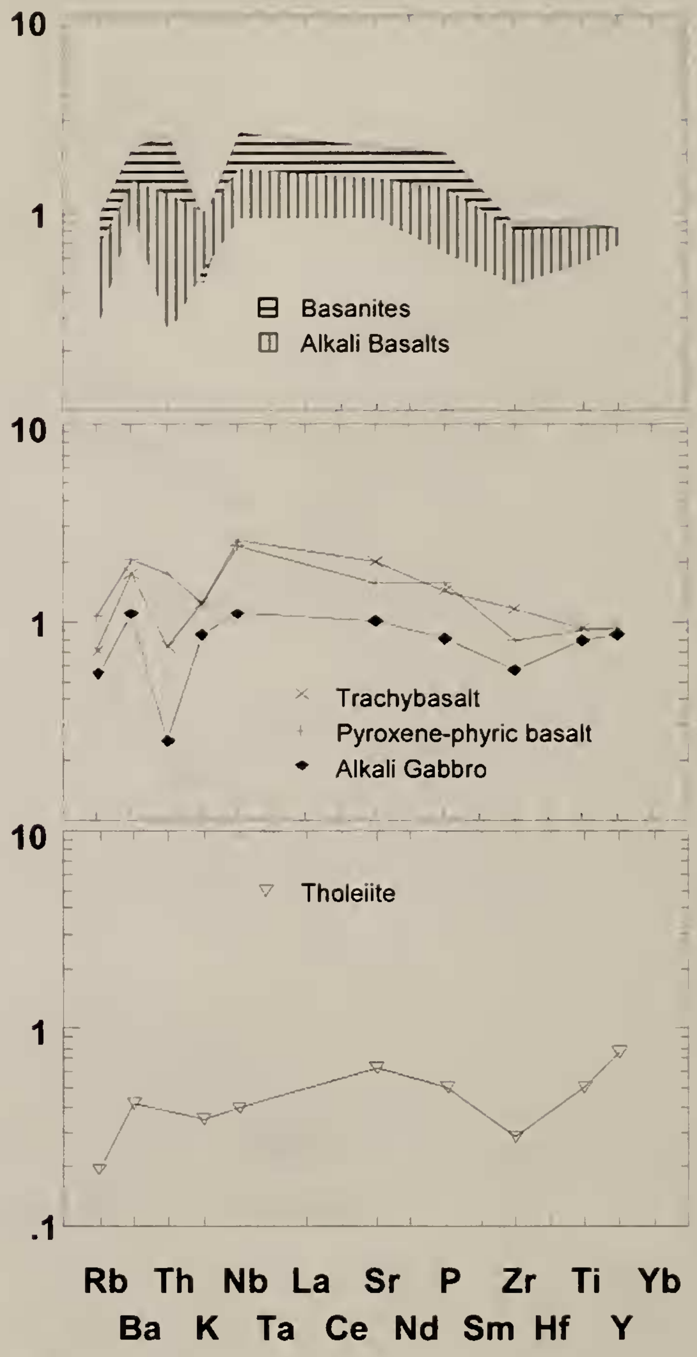

Figure 7 OIB-normalised multi-element plots of the various basaltic lithologies from the southern lava field. Normalisation values after Sun and Mc-Donough (1989).

could be due to plagioclase accumulation in these rocks as Zr is incompatible in this phase with respect to basaltic melts (Kd = 0.048; Rollinson 1993). Thus, the presence of excess plagioclase in the lavas may have diluted the bulk-rock Zr concentrations, hence the depletions.

TOWARDS A GENETIC MODEL

Mantle upwelling resulting in lithospheric melting via adiabatic decompression (eg. Hoernle et.al. 2006) is generally accepted as a likely mechanism for the generation of basaltic magmas in continental settings. Such a scenario (Fig. 9) is envisaged for the southern Barrington Tops lava field, where once formed, some of the magma ascended directly to the surface as evidenced by high-pressure (>1Gpa) gabbroic enclaves and reported mantle xenoliths (Powell and O'Reilly 2007). The majority of the magma, however, was stored in high crustal-level reservoirs conducive to the crystal fractionation of olivine + plagioclase, an assemblage characteristic of low pressure crystallisation. An internal build-up of water in the

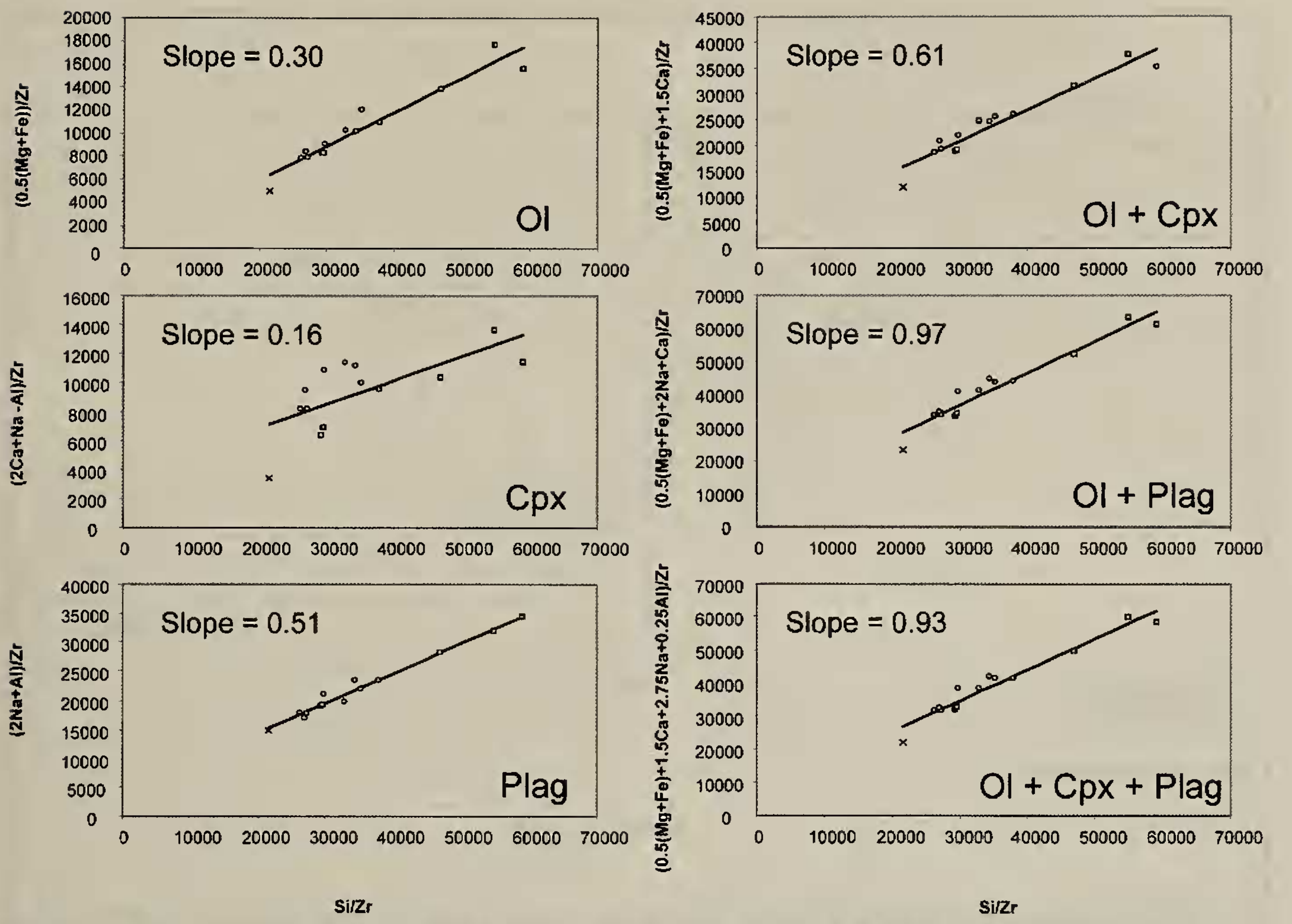

Figure 8. Pearce element ratio diagrams testing for various fractionation/accumulation controlled basaltic mineral assemblages. Note that Ol = Olivine; Cpx = Clinopyroxene; Plag = Plagioclase. Same symbols used as in Figure 4

system 'pushed' the cotectic into the clinopyroxene field. The late crystallisation of clinopyroxene may account for the observed phenocrysts in the rocks while obscuring it in the fractionation models. The alkali basalts, whilst free of clinopyroxene phenocrysts, also fractionated the mineral but in this case the pyroxene phenocrysts dropped completely out of the magma and accumulated on the floors and walls of the magma chambers where they continued to grow. Mason (1985) concluded in his study from the northern part of the field that the cores of these phenocrysts possibly crystallised as deep as the core/mantle boundary based on aluminium stoichiometry. Although similar polybaric crystallisation of pyroxene from ankaramites of the southern lava field (Bruce 1995) suggests shallower depths than this, it certainly does not preclude the existence of deeper level magma chambers, possibly feeding the upper crustal reservoirs. Eruption of these cumulates resulted in the proxene-phyric basalts, which in the field are stratigraphically associated with the alkali basalts. Stratigraphic relationships, magnetic anisotropy and chemical data are consistent with the genesis of the alkali gabbro as remnant dykes/plugs which necessitated the movement of the magma towards the surface.

GEODIVERSITY

The southern area of the Barrington Tops lava field has a topographic relief of about 1500m a.s.l whereas the floor of the incised valleys of the Allyn and Williams Rivers has an average elevation of 430m a.s.l. An escarpment marks the southern edge of the plateau. South of the plateau the region is dominated by the Mount Royal, Allyn and Williams Ranges. These ranges are partially capped with basalt while the valleys separating them are not and consist of folded Carboniferous sediments which form the bedrock for the Patterson, Allyn and Williams Rivers. Within these sedimentary units is a conglomerate that crops out along the Allyn River comprised of rounded pebble to boulder-sized granitoids, diorite, siltstones

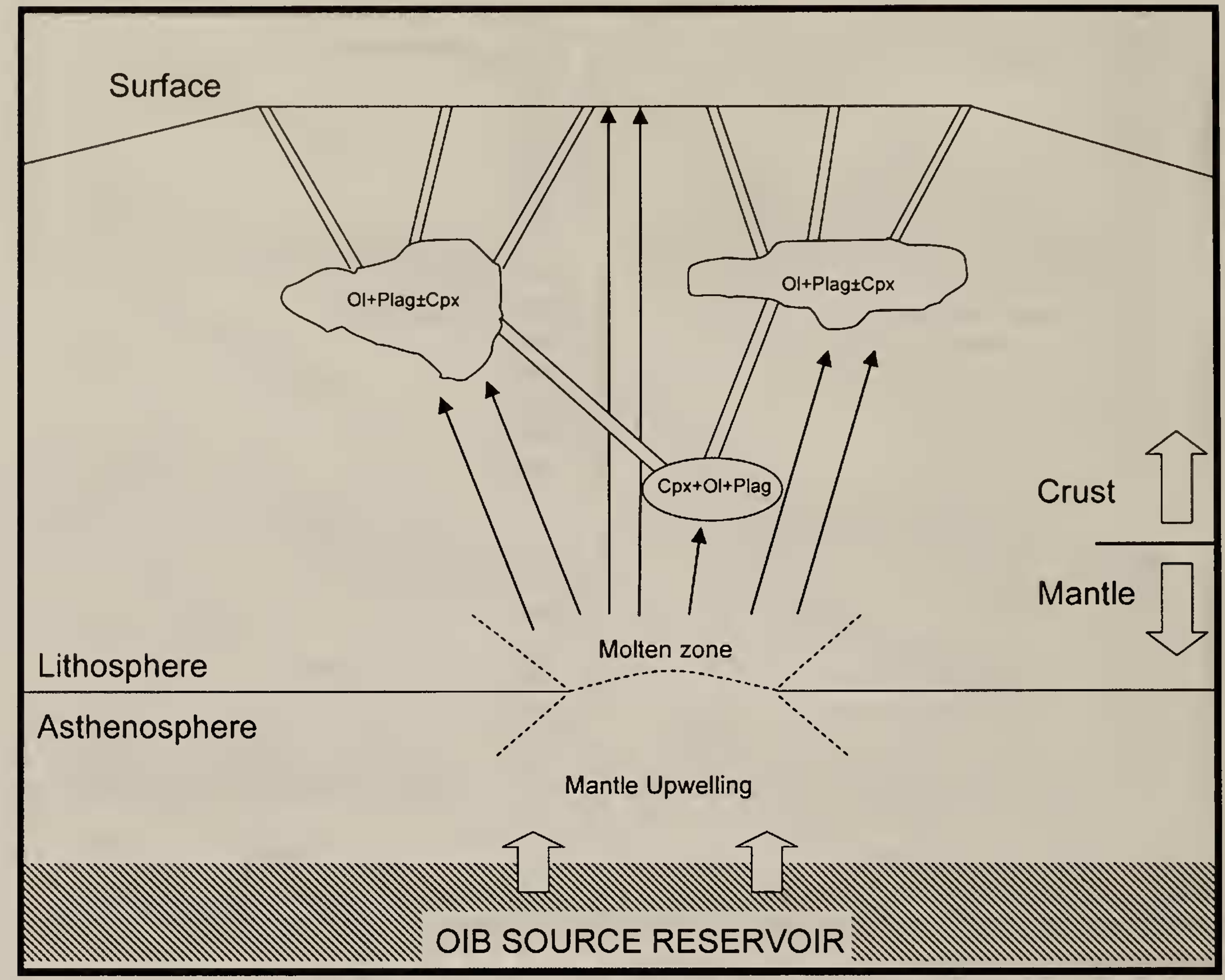

Figure 9. Schematic diagram illustrating the petrogenesis of the basaltic lavas. See text for details.

and quartzites cemented in a sandy matrix. Of particular note is the occurrence of an S-type granite clast similar in composition to parts of the Bathurst Batholith (S. Shaw pers. comm.). Rb/Sr dating on muscovite has returned an age of 325 ± 3.2 Ma (Bruce 1995), suggesting it may have been sourced from ~300 km to the south-west.

Basalt is present from the highest peak (Mount Barrington) down to an altitude of ~920m a.s.l. The resultant volcanic pile is thus ~630m thick. The basaltic flows are sub-horizontal based on the nature of palaeosols which would suggest that the pre-basalt surface consisted of a gently sloping topography. Pain (1983) envisaged a shield volcano for the lava field, an interpretation favoured by most authors (O'Reilly and Zhang 1995; Sutherland and Fanning 2001; Sutherland and Graham 2003). Nevertheless, there is evidence of some localised relief for the pre-basalt surface. Alignment of ferromagnetic minerals, defining lineations or foliations, in individual samples have dips of 20 degrees or more (Bruce 1995). A feature of the basalt today is that it is seen to cover the plateau and ridge tops and is absent in the deeply dissected valleys. This is the opposite of what would be expected had the flows formed on the current topography. It implies that subsequent to the eruption of the basalt, which filled up gently sloping valleys leaving ridges untouched, topographic inversion may have occurred due to a high rate of sedimentary erosion. The previously uncovered ridge tops, consisting of softer Carboniferous sediments, have eroded away to form valleys while the basalt filled valleys have resisted erosion to form the ridge tops. Evidence supporting this model includes the occurrence of a Cenozoic gravel deposit underlying basalt on the Williams Range (Bruce 1995). Such deposits (or deep leads) are indicative of buried valleys. Similar Cenozoic gravel deposits now situated on ridges have been reported by Mason (1982) from beneath the basalt from the western part of the lava field.

Erosion has dramatically altered the Barrington landscape since the Paleocene/Eocene basaltic eruptions in the southern part of the lava field. This has led to some impressive rock formations such as columnar basalt to be found on and around places like Mount Allyn and Mount Lumeah. The plateau and all its distinctive natural features is a post basalt erosional surface (Galloway 1967) and possibly represents remnants of scarp retreat of the Great Dividing Range (Ollier 1982). Rubies, sapphires and zircons of gem quality and rare secondary minerals are associated with the lava field (Sutherland and Graham 2003).

CONCLUSIONS

Geological mapping in the southern Barrington Tops lava field has identified 33 basaltic flows correlated from several localities over 630m of topographic relief. This matches the number of flows recorded by Mason (1982) albeit over only 430m of relief, in the Prospero Trigonometric station sequence in the north-western lava field. In the southern region, flows 10-20m thick are separated by either an agglomerate or sub-horizontal palaeosols. Petrography and whole-rock geochemistry reveal basanites dominate the lava sequence interspersed with alkali basalts, pyroxene-phyric basalts (ankaramites) and tholeiites. Alkali gabbros form intrusions near the top of the sequence and represent conduits for surface lavas. Major and trace elements of the alkaline magmas along with fractionation/accumulation controlled modelling are consistent with the magmas being co-genetic and chiefly controlled by a low pressure olivine + plagioclase mineral assemblage. Clinopyroxene did fractionate without greatly affecting magma compositions. Incompatible trace elements are consistent with low degree melting of an enriched mantle source (OIB-type), although there is evidence of entrained amphibole-enriched sub-continental lithospheric mantle. A third, more depleted mantle component, may have contributed to the tholeiites. These conclusions are consistent with alkali basalts analysed from the northern part of the lava field (O'Reilly and Zhang 1995; Sutherland and Fanning 2001) where basalt generation was linked to thermal anomalies in the mantle causing low degree asthenospheric and lithospheric melting. These melts rose up relatively quickly where they largely pooled in high crustal level magma chambers, fractionated olivine ± clinopyroxene and accumulated plagioclase before venting. The presence of peridotite xenoliths (Powell and O'Reilly 2007) suggests that at least some of the magma ascended directly from the upper mantle, sampling lower crustal material (gabbroic enclave) enroute to the surface.

ACKNOWLEDGEMENTS

Research for this project was undertaken in 1995 as partial requirements of a Bachelor of Science (Hons) Degree with the then School of Earth Sciences at Macquarie University, Sydney. Ian Percival and Trevor Green are thanked as principal supervisors whose guidance and discussions proved invaluable. Norm Pearson and Carol Lawson provided assistance with geochemical analysis. Jim Starling (NSW National Parks and Wildlife) and Mike Prima (NSW State Forests) gave permission to visit and sample localities at Barrington. I am grateful for reviews by Lin Sutherland and Suzanne O'Reilly that improved the final version of the manuscript. Published with the permission of the Acting Director, Geological Survey of New South Wales.

REFERENCES

Benson, W.N. (1912). Preliminary note on the nepheline-bearing rocks of the Liverpool and Mount Royal Ranges. *Journal and Proceedings of the Royal Society of New South Wales* **45**, 176-186.

Binns, R.A., Duggan, M.B. and Wilkinson, J.F.G. (1970). High pressure megacrysts in alkaline lavas from northeastern New South Wales. *American Journal of Science* **69**, 132-168.

Bruce, M.C. (1995). The petrology, geochemistry and origin of the Tertiary basalt from the southern Barrington Tops lava field, New South Wales. BSc (Hons) thesis, Macquarie University, Sydney.

Crawford, A.J., Stevens, B.P.J. and Fanning, M. (1997). Geochemistry and tectonic setting of some Neoproterozoic and Early Cambrian volcanics in western New South Wales. *Australian Journal of Earth Science* **44**, 831-852.

Eggins, S. (1984). Geology and geochemistry of the Barrington Tops Batholith. BSc (Hons) thesis, University of New South Wales, Sydney.

Galloway, R.W. (1967). Pre-basalt, sub-basalt and post-basalt surfaces of the Hunter Valley, New South Wales. In 'Landform studies from Australia and New Guinea' (Eds J.N. Jennings and J.A. Mabutt) pp 293-313. (Australian National University Press, Canberra).

Green, T.H. (1992). Petrology and geochemistry of basaltic rocks from the Balleny Isles, Antarctica. *Australian Journal of Earth Sciences* **39**, 603-617.

Hoernle, K., White, J.D.L., van der Bogaard, P., Hauff, F., Coombs, D.S., Werner, R., Timm, C., Garbe-Schonberg, D., Reay, A. and Cooper, A.F. (2006). Cenozoic intraplate volcanism on New Zealand: Upwelling induced by lithospheric removal. *Earth and Planetary Science Letters* **248**, 350-367.

Le Bas, M.J., Le Maitre, R.W., Streckeisen, A. and Zanettin, B. (1986). A chemical classification of volcanic rocks based on the total alkali-silica diagram. *Journal of Petrology* **27**, 745-750.

Mason, D.R. (1982). Stratigraphy of western parts of the Barrington Tops Tertiary volcanic field. In 'New England Geology: Voisey Symposium 1982' (Eds P.G. Flood and B. Runnegar) pp 133-139. (University of New England, Armidale, Australia).

Mason, D.R. (1985). Polybaric crystallisation of clinopyroxene in ankaramites of the Barrington Tops Tertiary volcanic field, New South Wales. *Geological Society of Australia, New South Wales Division Publication* **1**, 87-105.

Mason, D.R. and Kavalieris, I. (1984). A preliminary note on the Barrington Tops Granodiorite, New South Wales, Australia. *American Mineralogist* **71**, 1314-1321.

Middlemost, E.A.K. (1985). 'Magmas and magmatic rocks'. (Longman, London).

Norrish, K. and Hutton, J.T. (1969). An accurate X-ray spectrographic method for the analysis of a wide range of geological samples. *Geochimica Cosmochimica Acta* **33**, 431-453.

Norrish, K. and Chappell, B.W. (1977). X-ray fluorescence spectrometry. In 'Physical methods in determinative mineralogy' (Ed J. Zussman) pp 201-272. (Academic Press, London)

Ollier, C.D. (1982). The Great Escarpment of eastern Australia: tectonic and geomorphic significance. *Journal of the Geological Society of Australia* **29**, 36-43.

O'Reilly, S.Y. and Zhang, M. (1995). Geochemical characteristics of lava-field basalts from eastern Australia and inferred sources: connections with the subcontinental lithospheric mantle? *Contributions to Mineralogy and Petrology* **121**, 148-170.

Pain, C.F. (1983). Geomorphology of the Barrington Tops area, New South Wales. *Journal of the Geological Society of Australia* **30**, 187-194.

Pearce, T.H. (1968). A contribution to the theory of variation diagrams. *Contributions to Mineralogy and Petrology* **19**, 142-157.

Powell, W. and O'Reilly, S. (2007). Metasomatism and sulphide mobility in lithospheric mantle beneath eastern Australia: Implications for mantle Re-Os chronology. *Lithos* **94**, 132-147.

Roberts, D.L., Sutherland F.L., Hollis J.D., Kennewell P. and Graham, I.T. (2004). Gemstone characteristics North East Barrington Plateau, NSW. *Journal and Proceedings of the Royal Society of New South Wales* **137**, 99-122.

Rollinson, H. (1993). 'Using geochemical data: evaluation, presentation, interpretation'. (Longman Group Limited, UK).

Russell, J.K. and Nicholls, J. (1988). Analysis of petrological hypotheses with Pearce element ratios. *Contributions to Mineralogy and Petrology* **99**, 25-35.

Sun, S.S. and McDonough, W.F. (1989). Chemical and isotopic systematics of oceanic basalts: implications for mantle compositions and processes. In 'Magmatism in ocean basins' (Eds A.D. Saunders and M.J. Norry) pp 313-345. (Geological Society of London Special Publication **42**).

Sutherland, F.L. and Fanning, C.M. (2001). Gem-bearing basaltic volcanism, Barrington, New South Wales: Cenozoic evolution, based on basalt K-Ar ages and zircon fission track and U-Pb isotope dating. *Australian Journal of Earth Sciences* **48**, 221-237.

Sutherland, L. and Graham, I. (2003). 'Geology of Barrington Tops Plateau: Its rocks, minerals and gemstones, New South Wales, Australia'. (The Australian Museum Society, Sydney).

Wellman, P. (1989). Upper mantle, crust and geophysical volcanology of eastern Australia. In 'Intraplate Volcanism in eastern Australia and New Zealand' (Ed R.W. Johnson) pp 29-38. (Cambridge University Press, Cambridge).

Wellman, P., McElhinney, M.W. and McDougall, I. (1969). On the polar wander path for Australia during the Cainozoic. *Geophysical Journal of the Royal Astronomical Society* **18**, 371-395.

Table A1 Major and trace element XRF analyses, southern Barrington lava field.

Sample	MU55361	MU55365	MU55366	MU55369	MU55372	MU55378	MU55381	MU55382	MU55383
Barrington Tops 1:25k 9133-1-N	GR.492538	GR.500539	GR.553660	GR.502533	GR.553522	GR.528540	GR.520553	GR.524550	GR.553518
Rock type	Alkali basalt	Pyroxene-phyric basalt	Basanite	Alkali gabbro	Basanite	Basanite	Alkali basalt	Alkali basalt	Basanite
wt%									
SiO2	47.44	45.25	43.92	48.9	44.16	43.63	45.02	44.95	44.15
TiO2	1.97	2.55	2.31	2.3	2.53	2.44	2.36	2.46	2.35
Al2O3	14.49	16.01	14.27	16.38	14.54	13.25	14.82	14.87	14.7
Fe2O3	1.93	1.85	1.91	1.85	1.91	1.96	1.92	1.98	1.88
FeO	9.63	9.28	9.55	9.23	9.55	9.8	9.64	9.9	9.42
MnO	0.17	0.18	0.19	0.16	0.19	0.19	0.18	0.18	0.2
MgO	10.44	7.31	11.14	6.28	10.95	13.53	10.59	10.49	10.86
CaO	9.8	11.73	11.47	9.67	11.5	10.39	10.29	10.06	10.94
Na2O	2.72	3.32	3.38	3.28	2.98	2.97	3.05	3	2.6
K2O	1.11	1.77	0.68	1.24	0.85	0.64	1.42	1.48	1.34
P2O5	0.39	0.96	0.99	0.5	1.07	0.73	0.82	0.82	0.85
Total	100.09	100.21	99.81	99.79	100.23	99.53	100.11	100.19	99.29
ppm									
Ba	409	712	567	381	580	427	417	430	681
Rb	20	33	10	17	22	16	20	22	31
Sr	634	1017	1450	666	1146	917	889	989	1141
Y	20	27	24	25	23	22	24	25	23
Zr	122	226	194	158	246	188	231	233	177
Nb	46	115	79	53	103	85	79	81	79
Th	1	7	4	1	6	2	5	4	5
Pb	5	3	4	5	3	6	6	4	5
Ga	19	23	19	24	20	17	20	19	20
Zn	90	76	80	84	80	84	78	81	58
Cu	43	62	54	43	51	39	61	62	47
Ni	171	82	181	52	177	320	204	208	178
V	228	240	245	219	243	248	245	233	238
Cr	351	112	325	84	337	327	372	326	303

Sample	MU55385	MU55386	MU55393	MU55397	MU55401	MU55409	MU55411	MU55418	MU55424
Barrington Tops 1:25k 9133-1-N	GR.563513	GR.555492	GR.565516	GR.555490	GR.519466	GR.518458	GR.518444	GR.560480	GR.526441
Rock type	Basanite	Alkali basalt	Basanite	Trachybasalt	Basanite	Basanite	Basanite	Tholeiite	Alkali basalt
wt%									
SiO2	44.85	45.01	42.87	46.1	43.33	43.01	43.59	49.15	45.17
TiO2	2.28	2.19	2.15	2.65	2.25	2.45	2.38	1.49	1.61
Al2O3	14.41	14.8	13.73	15.97	14.1	13.87	13.35	16.42	13.49
Fe2O3	1.93	1.99	1.82	1.9	1.84	1.81	1.82	2.09	1.92
FeO	9.67	9.97	9.1	9.49	9.15	9.06	9.1	10.44	9.56
MnO	0.17	0.18	0.19	0.18	0.18	0.19	0.18	0.18	0.2
MgO	11.23	11.31	11.64	7.99	11.28	12.12	12.32	6.33	13.22
CaO	10.58	10.53	11.56	9.19	11.1	12.19	11.96	10.03	10.24
Na2O	2.59	2.5	3.67	3.32	3.31	2.78	2.72	2.77	2.69
K2O	0.81	0.95	0.96	1.78	0.93	0.76	0.81	0.52	0.75
P2O5	0.66	0.6	1.23	0.88	1.25	1.22	1.2	0.32	0.75
Total	99.18	100.03	98.92	99.45	98.72	99.46	99.43	99.74	99.6
ppm									
Ba	442	355	771	606	687	663	680	146	517
Rb	9	11	12	22	15	13	18	6	12
Sr	843	768	1322	1328	1330	1292	1413	412	776
Y	23	20	24	27	23	25	24	22	23
Zr	165	146	219	324	251	242	202	80	125
Nb	62	55	109	121	100	123	98	19	51
Th	3	2	10	3	6	4	4	0	5
Pb	4	5	6	2	3	5	5	3	4
Ga	18	19	17	19	15	15	16	21	14
Zn	75	80	77	83	74	73	73	80	78
Cu	64	67	45	33	43	53	42	71	65
Ni	224	213	252	107	206	198	239	208	388
V	212	222	225	195	205	256	245	192	210
Cr	312	318	372	115	361	367	366	294	542